Optics Letters

Artificial compound eye-tipped optical fiber for wide field illumination

Feng Liu,[1,3] **Qing Yang**,[2,3] **Hao Bian**,[1,3] **Fan Zhang**,[1,3] **Xun Hou**,[1] **Depeng Kong**,[4] and **Feng Chen**[1,3,*]

[1]State Key Laboratory for Manufacturing System Engineering and Shaanxi Key Laboratory of Photonics Technology for Information, School of Electronics & Information Engineering, Xi'an Jiaotong University, Xi'an, 710049, China
[2]School of Mechanical Engineering, Xi'an Jiaotong University, Xi'an, 710049, China
[3]International Joint Research Laboratory for Micro/Nano Manufacturing and Measurement Technologies, Xi'an Jiaotong University, Xi'an, 710049, China
[4]Key Laboratory of Transient Optics and Photonics, Xi'an Institute of Optics and Precision Mechanics, Chinese Academy of Sciences, Xi'an, 710119, China
*Corresponding author: chenfeng@mail.xjtu.edu.cn

Received 26 September 2019; accepted 7 November 2019; posted 11 November 2019 (Doc. ID 378866); published 5 December 2019

In this Letter, we present a novel, to the best of our knowledge, component with beam delivering and wide field beam homogenizing functions by grafting an artificial compound eye (ACE) micro-structure onto the polymer optical fiber (POF) end face. The 3D ACE mold is fabricated by femtosecond laser-assisted micro machining, and the ACE micro-structure is transferred onto the end face through high accuracy nano-imprinting. The resultant POF end face integrates over 400 spherical micro-lenses, enabling a 40% enhancement in both the acceptance angle and the effective numerical aperture. Meanwhile, the integrated ommatidia array serves as an outstanding beam homogenizer, shaping the output beam into quasi flat-top distribution, which demonstrates promise in wide field homogeneous illumination, by reflection and transmission imaging experiments in both visible and near infrared bands.

https://doi.org/10.1364/OL.44.005961

Wide field homogenous light beams are essential in emerging applications, such as biometric imaging in endoscopic and minimally invasive treatments [1–8], photothermal therapy [9], portable laser projection [10], speckle field imaging [1,11], and omnidirectional optical access [12]. In such applications, the acceptance/divergence angle and the intensity homogeneity are key features of the beam shaping component. Polymer optical fiber (POF) is a very flexible and cost-efficient light guide component with its large core and multimode operation, and it already plays an important role in extensive applications, such as short range optical communication [13], high precision sensing [14–16], and illumination light delivery [17]. But being limited by the core/cladding materials' indices, the numerical aperture (NA) value of the POF is ordinarily between 0.2 and 0.5, which severely limits the acceptance angle and the illumination field. Although several tip engineered fiber optics [18–20] based on the diffractive principle have been developed to shape the delivered beam [21–23], they may suffer from high loss and costly fabrications. The multimode fiber itself can be used as a beam shaping device [24], but it is difficult to meet the requirement in a plug-and-play scenario because of the complex adjustments by the waveguide length and the coupling strategy. In this work, the artificial compound eye (ACE) micro-structure was grafted onto the end face of the POF to enlarge the effective NA value of the POF and homogenize the output light beam. The artificial compound eye mold is fabricated by the femtosecond laser-assisted wet etching (FLWE) technique [25], and the featured 3D micro-structures are transferred onto the end face of the POF by nano-imprinting processing [26]. The fabricated POF end face is close-packed with hundreds of spherical micro-lenslets with the diameter of 85 μm on a macro dome morphology with a radius of curvature (RoC) of 2.5 mm, and the micro-elements' fill factor approaches 100%. The measured acceptance angle of the ACE-tipped POF reaches 81°, indicating the enlarged NA of 0.65. The homogeneity of the output beam is confirmed by the radial visibility evaluation and the imaging experiments with homogenized illumination in both visible and NIR bands. Such a proposed component would find potential applications in high-performance biomedical illumination, omnidirectional optical link access, and so on.

The fabrication of the ACE-tipped POF starts from a hard concave 3D ACE mold which is prepared by a high-efficient maskless FLWE technique on a curved BK7 borosilicate optical glass substrate. Our previous articles have shown that such manufacturing can have great flexibility and precision control in the final morphology by tailoring the laser implantation conditions, including irradiation laser pulse energy [27,28], exposure time [27,28], focus offset [29,30], and laser polarization [30]. The femtosecond laser pulses from a Ti:sapphire regenerative amplifier (Institute of Physics, CAS, Harmonic Laser) are focused onto the substrate surface and irradiate the glass with the implantation dose of 425 $\mathrm{kJ/cm^2}$ per site. The

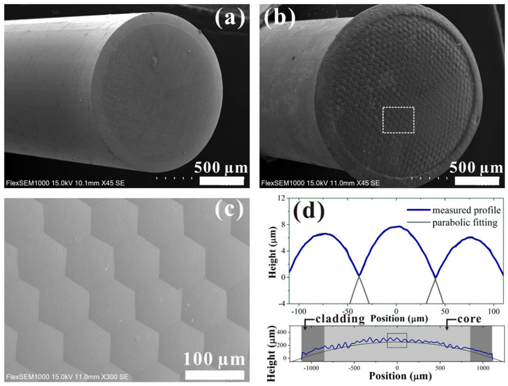

Fig. 1. (a) Polished original planar POF end face. (b) Fabricated ACE-featured POF end face. (c) Zoomed details of the ommatidia [in the dashed box in (b)]. (d) Cross section profile of the ACE end face and the details at the central part (indicated by the dashed box).

site-by-site photon implantations are performed in a hexangular array scheme with the separation of 85 μm by moving the sample in the $x-y$ plane. Then, the laser-induced volumetric modification zone is selectively etched down and polished by chemical etchant. Finally, a hard concave ACE mold with macro dome morphology (with a base radius of 2.5 mm and sagitta of 1.45 mm) and nanometer scale surface roughness is formed. The whole procedure to prepare such a hard mold takes about 2 h by using the optimized fabrication parameters. Considering the massive units integrated in the mold, to form a single perfect micro optical surface only takes 2 s through the FLWE technique, which shows great advantage in fabrication efficiency.

The featured convex ACE micro-structure on the POF end face is prepared by 3D nano-imprinting above the heat deflection temperature (HDT) [31] of the polymer material. A homemade step index POF with a core diameter of 1.6 mm (polymethyl methacrylate, PMMA, with refractive index of 1.49, HDT at 1.8 MPa of 97°C) and a fluorinated polymer cladding with thickness of 120 μm (polyvinylidene fluoride, PVDF, with refractive index of 1.42, and HDT at 1.8 MPa of 115°C) is chosen to fabricate the ACE-tipped component. A piece of such POF with a cleaved and finely polished end face [as shown in Fig. 1(a)] is mounted on a stage driven by a stepping motor (PI, M-L01.2S0), while the mold is placed beneath the stage on an electric hot plate. The mold is heated to 110°C with temperature increment of 4°C/min. Then, a mechanical pressure of 1.4 MPa is applied onto the POF in a vertical direction and kept for 150 s. After that, the whole module is cooled down in the ambient air, then the fabricated component is demolded.

The fabricated ACE-tipped POF end face is shown in Fig. 1(b), and the detailed ommatidia feature is shown in Fig. 1(c). The micro-structures are only presented inside the core region, due to the different HDTs of the core and the cladding materials in the processing condition ($HDT_{core} < T_{processing} < HDT_{cladding}$). The profile by the laser scanning confocal microscope (LSCM, Olympus, LEXT OLS4000) measurement is shown in Fig. 1(d), the macro dome morphology with a RoC of 2.5 mm is packed with ommatidium units with diameters of 85 μm, sag heights of 8 μm, and surface roughnesses of 60 nm ($\lambda/10$ at 633 nm).

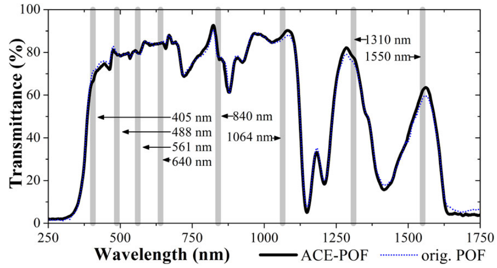

Fig. 2. Transmittances of the fabricated ACE-tipped POF sample and its original counterpart.

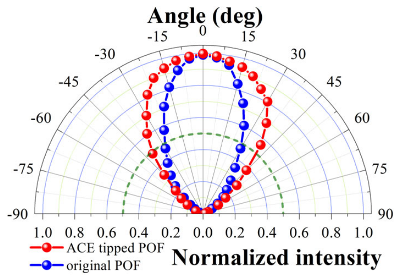

Fig. 3. Normalized angular intensity distributions measured with both an ACE-tipped POF and its original counterpart.

A piece of an ACE-tipped POF sample with a length of 150 mm and its original counterpart are used to evaluate the optical loss. The transmittance of the fabricated sample is characterized with an UV-Vis-NIR spectrophotometer (PerkinElmer, Lambda 750) equipped with an integrating sphere detector, as shown in Fig. 2. As the imprinting temperature is well controlled, there is no composition modification around the fabrication area, so there is no obvious change in the transmission spectrum. The fabricated sample shows relatively high transparency in the whole visible band and several discrete NIR windows, especially some technologically important wavelength bands, such as 405, 488, 561, and 640 nm for fluorescence excitation, 840 nm, 1064 nm, and 1310 nm for optical coherence tomography (OCT), 1550 nm for high capacity optical link, and so on. The optical attenuation loss is estimated as 2.3 dB/m in most optical windows. The two major absorption dips at 1.2 and 1.4 μm are due to the overtones of the C-H vibrations [32]. Such remarkable spectral transparency combining with a very high core ratio (75%) makes the prepared sample extremely suitable for short range light delivery with massive power.

The ACE-structured POF end face would result in an enlarged acceptance angle due to the basic principle of enlarged field of view (FoV) of the 3D compound eye structure [33]. The acceptance angle is experimentally measured by collimated beam input coupling with a He–Ne laser (DH-HN150, with wavelength of 633 nm, output power of 2.8 mW, and beam width of 0.6 mm). The laser source is mounted on a radially scanning stage whose center is overlapped with the ACE-structured input facet. The output laser power is recorded with a photodiode powermeter (Ophir Photonics, PD300R). The normalized radial power distribution is shown in Fig. 3. By comparing it with the result from an original POF, the full acceptance angle (defined at the FWHM intensity, as marked with a dash line) is enlarged from 57° to 81°, by a numerical increment of 42%. The NA values are calculated by the definition for multimode fiber optics [34], as

$$\mathrm{NA} = n \sin \theta_{\mathrm{acc}}, \tag{1}$$

where the surrounding refractive index n takes unit value as in the open air operation condition, and θ_{acc} is the acceptance angle defined as the angle between the maximum incidental direction and the axial direction of the fiber. The calculated NA values are enlarged from 0.47 to 0.65, by a numerical increment of 38%. Such property shows great advantage in light collection with very wide field, and the ACE-enhanced POF component would find application in omnidirectional optical signal picking, such as wide field access in high capacity omnidirectional optical link terminals and biomedical fluorescence signal picking [35,36].

Such a micro-structured device also predicts its potential as an outstanding integrated homogenizer light guide device. The ACE-structured end face divides the output light beam into a beamlets array, and then the micro-beamlets overlap in the space, which transforms the light intensity to a flat-top-like profile in the far field. Hence, such refractive micro-element arrayed diffusers exhibit independence from the incidental intensity profile, which is especially suitable for the polymer multimode fibers which carry a large amount of modes. A traditional solid diffuser component which is inserted into the light path would cause at least 7.5% (0.34 dB) loss due to the Fresnel reflection [37], but this loss could be avoided by our proposed integrated component. The ACE-tipped POF with a length of 480 mm is chosen to investigate the beam-homogenizing performance. The central part of the fiber is periodically steered by six rods with a diameter of 12.7 mm and a separation of 50 mm, forming a mode scrambler to build up the equilibrium mode distribution within the limited length [38], and the beam from the He–Ne laser is coaxially launched into the POF samples. The output light illuminates a blank screen 20 cm away from the output facet. The measured intensity profile of the illumination area is compared with the one from an original POF sample, as shown in Fig. 4.

The quasi hat-top and Gaussian-like output distributions are both fitted with a super Gaussian equation [39], as

$$I(r) = I_0 e^{-2(r/w_0)^n}, \tag{2}$$

in which the I_0 is the peak intensity, r is the radial position, and w_0 is equivalent beam waist. The fitted parameters are listed in Table 1.

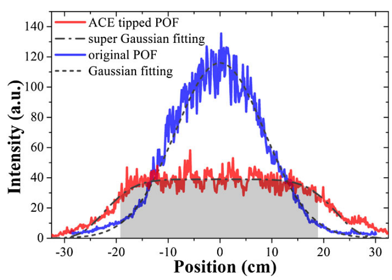

Fig. 4. Measured intensity distributions of the delivered light from an ACE-tipped POF and the original POF counterpart. The grey shadow indicates the ROI for evaluating the degree of inhomogeneity.

Table 1. Fitted Parameters for the Measured Profiles

	ACE-Tipped POF (Quasi Flat-Top)	Original POF (Gaussian Like)
I_0	39	116
w_0	26	17.3
n	6	2

The degree of inhomogeneity could be expressed as $D = \sigma / I_{\mathrm{mean}}$, where σ is the standard deviation in the region of interest (ROI, defined as the region in which 85% of total light power is included), and I_{mean} is the average intensity. The D value with our ACE-tipped POF is measured as 0.13. The inhomogeneity of such an integrated beam is mainly from the laser speckles. The homogeneity could be further improved with a rotating diffuser or a vibrating diffuser [40] in the input light path, or using an incoherent light source, which both reduce the spatial coherence of the beam.

The imaging tests with homogeneous illumination by the structured POF sample are demonstrated by both reflection and transmission scenarios. The visibility is measured with the Michelson definition [41], as

$$V = \frac{L_{\mathrm{B}} - L_{\mathrm{D}}}{L_{\mathrm{B}} + L_{\mathrm{D}}}, \tag{3}$$

where L_B and L_D are the luminance values of the bright and dark regions, respectively. A checkerboard featured Lambertian target is illuminated from 50 mm away with the incoherent white light from a LED lamp by the POF's delivery, as shown in Fig. 5(a). The measured radial visibilities are shown in Fig. 5(b) for both POF samples, by empirical criterions of 0.2 (for machine vision) and 0.5 (for human vision). The ACE-tipped POF shows a larger legible region than the original one, which also coincides with the light intensity distribution in Fig. 4 very well. A plant tissue material (leaf of *Platanus orientalis*, water content of 56%) is chosen to demonstrate the transmission imaging with the homogenized NIR beam illumination. The cw laser beam with a wavelength of 1064 nm and an average power of 1.8 mW (CNI Inc., MSL-S-1064-S) is guided with an ACE-tipped POF sample and illuminates the leaf from 5 mm away. A Si CCD (Nikon, DS-Fi2) with a NIR pass filter (Teijin, Panlite LN-2250Y, 780 nm–2.2 μm) is used to capture the transmission images. The captured image with the ACE-tipped POF operation shows relatively uniform illumination in the main region of the FoV, for example, as shown in Fig. 5(c), the region with 85% of entire light density is illustrated with a dashed circle, in which the micro veins with thickness of 100 μm could be well identified. Compared with this, the beam delivered by the original POF [Fig. 5(d)] shows narrower FoV. In this scenario, with the same illumination power inside the 85% of the entire light density region (the dashed circle), the central part of the detector array is overexposed, while the periphery parts are underexposed, and a large amount of details in both the central region and the circumambient region of the target are lost.

In conclusion, a micro-structured ACE was integrated onto the end face of a POF by FLWE and nano-imprinting technique. The manufacturing strategy is efficient and flexible. The end face of the fabricated POF sample is close-packed with over 400 micro-lenslets, enabling an enlarged acceptance

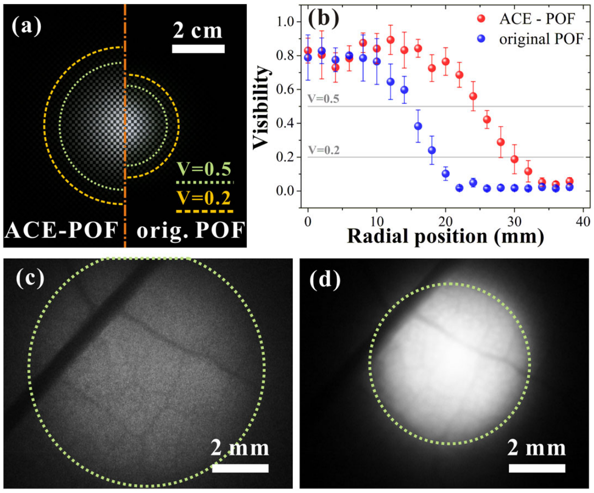

Fig. 5. (a) Checkerboard target illuminated by ACE-tipped POF samples and its original counterpart. (b) Measured visibilities for two illumination conditions. The transmission images of the leaf sample with NIR illumination beam delivered by (c) the ACE-tipped POF and (d) the original POF.

emitting angles. By serving as a refractive integral homogenizer, the micro-structured end face can effectively improve the uniformity of the output beam profile in a wide field. The imaging experiments and the visibility evaluation in both reflection and transmission schemes with the homogenized beam from the fabricated sample predict its potential applications in both visible and NIR bands, such as high-performance biomedical illumination, omnidirectional optical link terminal, and so on.

Funding. National Natural Science Foundation of China (11504416, 61435005, 61875158, U1630111); National Key Research and Development Program of China (2017YFB1104700); China Postdoctoral Science Foundation (2018M633499); Fundamental Research Funds for the Central Universities.

Acknowledgment. We thank the Instrument Analysis Center of Xi'an Jiaotong University. The SEM work was done at the International Center for Dielectric Research (ICDR), Xi'an Jiaotong University.

Disclosures. The authors declare no conflicts of interest.

REFERENCES

1. M. Plöschner, T. Tyc, and T. Čižmár, Nat. Photonics **9**, 529 (2015).
2. Y. Choi, C. Yoon, M. Kim, T. D. Yang, C. Fang-Yen, R. R. Dasari, K. J. Lee, and W. Choi, Phys. Rev. Lett. **109**, 203901 (2012).
3. B. Paulson, S. Lee, Y. Kim, Y. Moon, and J. K. Kim, Biomed. Opt. Express **10**, 2264 (2019).
4. Y. Zhang, Y. Cao, and J.-X. Cheng, Opt. Lett. **44**, 3841 (2019).
5. A. M. Caravaca-Aguirre and R. Piestun, Opt. Express **25**, 1656 (2017).
6. A. Ventura, F. B. Slimen, J. Lousteau, N. White, A. Masoudi, P. Janicek, and F. Poletti, Opt. Express **27**, 20259 (2019).
7. R. He, C. Liu, Z. Zhang, and J. Sun, OSA Continuum **2**, 839 (2019).
8. Y. Hu and K. Masamune, Opt. Express **25**, 16795 (2017).
9. L. L. Colombo, S. I. Vanzulli, A. Blázquez-Castro, C. S. Terrero, and J. C. Stockert, Biomed. Opt. Express **10**, 2932 (2019).
10. Y. Liu, D. Cheng, T. Yang, and Y. Wang, Opt. Express **27**, 12264 (2019).
11. U. Kürüm, P. R. Wiecha, R. French, and O. L. Muskens, Opt. Express **27**, 20965 (2019).
12. X. Xu, L. Ma, Y. Shi, T. Ishigure, and Z. He, Opt. Express **27**, 22419 (2019).
13. F. Shi, N. Bamiedakis, P. P. Vasil'ev, R. V. Penty, I. H. White, and D. Chu, J. Lightwave Technol. **36**, 2685 (2018).
14. X. Cheng, J. Bonefacino, B. O. Guan, and H. Y. Tam, Opt. Express **26**, 14610 (2018).
15. F. Zhang, X. Xu, J. He, B. Du, and Y. Wang, Opt. Lett. **44**, 2466 (2019).
16. A. Leal-Junior, A. Frizera, M. J. Pontes, P. Antunes, N. Alberto, M. F. Domingues, H. Lee, R. Ishikawa, Y. Mizuno, K. Nakamura, P. André, and C. Marques, Opt. Lett. **43**, 1754 (2018).
17. R. D. Breukers, G. J. Smith, H. L. Stirrat, A. J. Swanson, T. A. Smith, K. P. Ghiggino, S. G. Raymond, N. M. Winch, D. J. Clarke, and A. J. Kay, Appl. Opt. **56**, 2630 (2017).
18. H. Kim, J. Kim, H. An, Y. Lee, G. Lee, J. Na, K. Park, S. Lee, S.-Y. Lee, B. Lee, and Y. Jeong, Opt. Express **25**, 30290 (2017).
19. D. Duan, G. X. Du, V. K. Kavatamane, S. Arumugam, Y.-K. Tzeng, H.-C. Chang, and G. Balasubramanian, Opt. Express **27**, 6734 (2019).
20. N. Wang, M. Zeisberger, U. Hübner, and M. A. Schmidt, Opt. Mater. Express **8**, 2246 (2018).
21. C. Xu, K. Yan, C. Gu, P. Yao, L. Xu, and Q. Zhan, Opt. Lett. **43**, 1247 (2018).
22. H. Lee, J. Park, and K. Oh, J. Lightwave Technol. **37**, 2590 (2019).
23. A. V. Andrianov, N. A. Kalinin, M. Yu. Koptev, O. N. Egorova, A. V. Kim, and A. G. Litvak, Opt. Lett. **44**, 303 (2019).
24. X. Zhu, A. Schülzgen, H. Li, H. Wei, J. V. Moloney, and N. Peyghambarian, Opt. Express **18**, 7506 (2010).
25. H. Bian, Y. Wei, Q. Yang, F. Chen, F. Zhang, G. Du, J. Yong, and X. Hou, Appl. Phys. Lett. **109**, 221109 (2016).
26. Z. He, Y. Lee, R. Chen, D. Chanda, and S. Wu, Opt. Lett. **43**, 5062 (2018).
27. H. Bian, H. Liu, F. Chen, Q. Yang, P. Qu, G. Du, J. Si, X. Wang, and X. Hou, Opt. Express **20**, 12939 (2012).
28. F. Chen, H. Liu, Q. Yang, X. Wang, C. Hou, H. Bian, W. Liang, J. Si, and X. Hou, Opt. Express **18**, 20334 (2010).
29. X. Meng, F. Chen, Q. Yang, H. Bian, H. Liu, P. Qu, Y. Hu, J. Si, and X. Hou, IEEE Photon. Technol. Lett. **25**, 1336 (2013).
30. S. Tong, H. Bian, Q. Yang, F. Chen, Z. Deng, J. Si, and X. Hou, Opt. Express **22**, 29283 (2014).
31. "Plastics—determination of temperature of deflection under load—part 1: general test method," ISO 75-1:2013 (2013).
32. T. Kaino, in *Encyclopedia of Polymeric Nanomaterials*, S. Kobayashi and K. Müllen, eds. (Springer-Verlag, 2014).
33. X. Q. Liu, S. N. Yang, L. Yu, Q. D. Chen, Y. L. Zhang, and H. B. Sun, Adv. Funct. Mater. **29**, 1900037 (2019).
34. S. Werzinger, C.-A. Bunge, S. Loquai, and O. Ziemann, J. Lightwave Technol. **31**, 2769 (2013).
35. N. Wang, M. Zeisberger, U. Hübner, and M. A. Schmidt, ACS Photon. **6**, 691 (2019).
36. Y. Xue, K. P. Berry, J. R. Boivin, C. J. Rowlands, Y. Takiguchi, E. Nedivi, and P. T. C. So, Optica **6**, 76 (2019).
37. M. Ai, W. Shu, T. Salcudean, R. Rohling, P. Abolmaesumi, and S. Tang, Opt. Express **25**, 17713 (2017).
38. R. Attia and J. Marcou, Opt. Eng. **39**, 299 (2000).
39. K. Gillen-Christandl, G. D. Gillen, M. J. Piotrowicz, and M. Saffman, Appl. Phys. B **122**, 131 (2016).
40. Z. Deng, Q. Yang, F. Chen, H. Bian, J. Yong, G. Du, Y. Hu, and X. Hou, IEEE Photonics Technol. Lett. **26**, 2086 (2014).
41. E. Peli, J. Opt. Soc. Am. A **7**, 2032 (1990).